LATTICE BOLTZMANN AUTOMATON MODEL TO SIMULATE FLUID FLOW IN SYNTHETIC FRACTURES

A THESIS SUBMITTED TO
THE GRADUATE SCHOOL OF NATURAL AND APPLIED SCIENCES
OF
MIDDLE EAST TECHNICAL UNIVERSITY

BY

ERDİNÇ EKER

IN PARTIAL FULFILLMENT OF THE REQUIREMENTS
FOR
THE DEGREE OF MASTER OF SCIENCE
IN
PETROLEUM AND NATURAL GAS ENGINEERING

JANUARY 2005

Approval of the Graduate School of Natural and Applied Sciences.

_____

Prof. Dr. Canan Özgen
Director

I certify that this thesis satisfies all the requirements as a thesis for the degree of Master of Science.

_____

Prof. Dr. Birol Demiral
Head of Department

This is to certify that we have read this thesis and that in our opinion it is fully adequate, in scope and quality, as a thesis for the degree of Master of Science.

_____

Assoc. Prof. Dr. Serhat Akın
Supervisor

Examining Committee Members

Prof. Dr. Birol Demiral	(METU, PETE)	_____
Assoc. Prof. Dr. Serhat Akın	(METU, PETE)	_____
Prof. Dr. Fevzi Gümrah	(METU, PETE)	_____
Prof. Dr. Mustafa. V. Kök	(METU, PETE)	_____
M.Sc, Kubilay Kumsal	(Türkiye Petrolleri Ano. Ort.)	_____

I hereby declare that all information in this document has been obtained and presented in accordance with academic rules and ethical conduct. I also declare that, as required by these rules and conduct, I have fully cited and referenced all material and results that are not original to this work.

Name, Last name: Erdinç Eker

Signature :

ABSTRACT

LATTICE BOLTZMANN AUTOMATON MODEL TO SIMULATE FLUID FLOW IN SYNTHETIC FRACTURES

EKER, Erdinç

M.Sc, Department of Petroleum and Natural Gas Engineering

Supervisor: Assoc. Prof. Dr. Serhat Akın

January 2005, 57 pages

Modeling of flow in porous and fractured media is a very important problem in reservoir engineering. As for numerical simulations conventional Navier-Stokes codes are applied to flow in both porous and fractured media. But they have long computation times, poor convergence and problems of numerical instabilities. Therefore, it is desired to develop another computational method that is more efficient and use simple rules to represent the flow in fractured media rather than partial differential equations. In this thesis Lattice Boltzmann Automaton Model will be used to represent the single phase fluid flow in two dimensional synthetic fractures and the simulation results obtained from this model are used to train Artificial Neural Networks. It has been found that as the mean aperture-fractal dimension ratio increases permeability increases. Moreover as the anisotropy factor increases permeability decreases with a second order polynomial relationship.

Keywords: Lattice Boltzmann Automaton Model, Cellular Automata, Synthetic Fracture Generation, Simulation of Fluid Flow, Artificial Neural Networks.

ÖZ

BOLTZMANN KAFES OTOMAT MODELİ İLE SENTETİK ÇATLAKLARDA SIVI AKIŞ SİMÜLASYONU

EKER, Erdinç

Yüksek Lisans, Petrol ve Doğalgaz Mühendisliği Bölümü

Tez Yöneticisi: Doç. Dr. Serhat Akın

Ocak 2005, 57 sayfa

Gözenekli ve çatlaklı ortamlarda akış modellenmesi rezervuar mühendisliği alanında oldukça önemli bir problemdir. Bu ortamlardaki akış modellenmesi hesaplarında geleneksel Navier-Stokes denklemleri kullanılmaktadır, fakat bu yöntemin uzun hesaplama süresi, zayıf yakınsama ve sayısal kararsızlıklar gibi problemleri mevcuttur. Bu yüzden kısmi diferansiyel denklemler yerine çatlaklı ortamda sıvı akışını modellemek için basit kurallara dayalı bir yöntemin geliştirilmesi arzulanır. Bu tez Boltzmann Kafes Otomata Modeli ile iki boyutlu sentetik çatlaklarda tek fazlı akış gösterimi ve Yapay Sinir Ağlarının bu modelden elde edilen simülasyon sonuçlarıyla eğitilmesini kapsamaktadır. Çalışma sonunda çatlaklardaki ortalama aralık – fraktal boyutu oranının geçirgenlikle doğru orantılı olduğu ve anizotropi faktörü ile geçirgenliğin ikinci dereceden polinom ilişki ile ters orantılı olarak birbirlerine bağlı oldukları anlaşılmıştır.

Anahtar Kelimeler: Boltzmann Kafes Otomat Modeli, Hücresel Otomata, Sentetik Çatlak Oluşturulması, Sıvı Akışının Simülasyonu, Yapay Sinir Ağları.

To My Family

ACKNOWLEDGEMENTS

I want to express my sincere gratitude to my supervisor Assoc. Prof. Dr. Serhat Akın for his guidance and insight throughout the thesis study.

I would like to thank to my parents and sister for their patience during this rigorous and long work.

TABLE OF CONTENTS

LIST OF TABLES

TABLES

LIST OF FIGURES

FIGURES

LIST OF SYMBOLS

h	Fracture Aperture	mm
f	Surface Roughness Factor	dimensionless
k_{abs}	Absolute Permeability	md
ρ	Fluid Density	g / cm^3
u	Fluid Velocity	cm / sec
μ	Dynamic Viscosity	cp
ΔP	Pressure Difference	atm
r	Radius of the Pipe	mm
Ω	Collision Operator	dimensionless
L	Length of the Tube	mm
A	Anisotropy Factor	dimensionless
Q	Flow Rate	cm^3 / sec
τ	Relaxation Time	dimensionless

LIST OF ABBREVATIONS

LBM	Lattice Boltzmann Method
ANN	Artificial Neural Network
CFD	Computational Fluid Dynamics
LGA	Lattice Gas Automata
CA	Cellular Automata
BGK	Bhatnagar-Gross-Krook
PDE	Partial Differential Equation
FEM	Finite Element Method
FDM	Finite Difference Method
FVM	Finite Volume Method
MSE	Mean Square Error

CHAPTER 1

INTRODUCTION

Fractures play an important role in reservoir engineering as they dominate the fluid flow in the reservoir. The most important property of the reservoir rock is the absolute permeability, which is defined as the measure of the capacity of the medium to transmit fluids [1]. Because of this reason, determination of fracture permeability is very important to predict the performance of the reservoir.

A fracture is usually assumed as a set of smooth parallel plates separated by a constant width. The absolute permeability of a smooth-walled fracture is related to the fracture aperture using the cubic law. However, the flow characteristics of an actual fracture surface would be quite different, affected by tortuosity and surface roughness. Though several researchers as Witherspoon et al. [2], and Walsh et al. [3], have discussed the effect of friction on flow, a unified methodology for studying flow on a rough fracture surface has not emerged.

In the past single phase fluid flow through a fracture was described by Poiseuille flow between two parallel and smooth plates. The separation between them is defined as fractures aperture h and the absolute permeability k_{abs} is defined as [4].

$$k_{abs} = \frac{h^2}{12} \tag{1.1}$$

But as this equation does not represent the surface roughness of a real fracture. Modifications were performed to consider the effect of surface roughness to the fracture permeability [2], where f is defined as the surface roughness factor.

$$k_{abs} = \frac{h^2}{(12f)} \tag{1.2}$$

These empirical relations only give an approximate result for the permeability calculations and as experimental methods are expensive and time consuming most of the time numerical methods are used. Most common numerical techniques are Finite-Element Method (FEM), Finite-Difference Method (FDM) and Finite Volume Method (FVM). The objective of all these methods is to transform the problem posed through partial differential equations to one having an algebraic representation [5].

Lattice Boltzmann Automaton Model, or with its more commonly used name, Lattice Boltzmann Method (LBM), was developed as another computational method based on Cellular Automata (CA) theory. This novel numerical method is more efficient especially in porous and fractured media and use simple rules to represent the fluid flow rather than partial differential equations [6]. According to the comparison studies between classical numerical methods like finite volume method and the lattice Boltzmann method, it was concluded that for fluid flow in complex geometries there appears to be a break-even point, where at a certain complexity of the geometry, the lattice Boltzmann method becomes more efficient than the finite volume method [7]. This makes the LBM a good candidate for the simulation studies in complex geometries like porous and fractured media.

LBM is a discrete computational method based upon the Boltzmann equation. It considers a typical volume element of fluid to be composed of a collection of particles that are represented by a particle velocity distribution

function at each grid point. In discrete time steps the fluid particles can collide with each other as they move. The rules that govern the collisions of the particles are designed such that the time averaged motion of the particles is consistent with the Navier-Stokes equation [6]. The complex geometric details in the porous media and fractures can be handled in terms of simple bounce-back rules.

In this thesis, results of the numerical computations for single phase flow simulations through two-dimensional synthetically created fracture apertures were presented. These synthetic rock fractures are created using different fractal dimensions, anisotropy factors, and mismatch lengths. Lattice Boltzmann method, was then used to determine the absolute permeability of different fracture apertures. Regions of high velocity and low velocity flow were identified. Artificial Neural Networks (ANN's) are trained with the outputs of the LBM simulations to understand the relationships between the fracture parameters and the absolute permeability of the fracture apertures. Mean square error values for both training and validation phases are small and indicate that the trained ANN could be used for future permeability predictions.

CHAPTER 2

BACKGROUND INFORMATION

2.1. Introduction

Fluid dynamics, which studies the fluids in motion, is one of the oldest and broadest fields of engineering. It has various branches and used nearly in all phases of engineering design and analysis. Computational Fluid Dynamics (CFD) is one of the branches of fluid dynamics and uses computational technology that enables engineers to study the dynamics of fluids with the aid of high performance computers and specialized algorithms [8]. In CFD, a model is built that represents the system that is being studied. Then the theory of fluid flow is applied to this model by using suitable formulas and algorithms. The results obtained can be used to predict the flow inside the model that is being studied and used for practical engineering purposes such as design of a new car engine or calculation of the contamination rate in an underground nuclear waste disposal area. CFD uses high-speed parallel computer architectures and numerical methods to find the solutions to the mathematical equations that describe fluid flow. It allows engineers to predict the results of their decisions in fluid flow problems and creates a simulation environment in which they can see the results of their decisions before it is applied in the real world. The approach in CFD is to start with Navier-Stokes equations. The Navier-Stokes equations are set of partial differential equations that statistically describe a real fluid. These equations are very complex and

highly non-linear; they cannot be solved analytically except for the simple problems.

More than a decade ago, the lattice-gas automata (LGA) and the lattice Boltzmann method (LBM) were proposed as alternatives for computational fluid dynamics [9]. The approach used to solve fluid flow problems in these methods is significantly different from the approach used in traditional CFD codes. The main difference is that while traditional CFD approaches start with a mathematical description of a fluid at the continuum level, i.e. the Navier-Stokes equations. Lattice Boltzmann method simulates fluids at a more fundamental, or kinetic level, with the discrete Boltzmann equation. The Boltzmann equation governs the dynamics of particle density functions [10].

Fluid flow through porous and fractured media is a specific fluid mechanical application of great practical value in applied science and engineering. Most difficult problems in fluid dynamics arise in porous and fractured media because of their geometrical complexity. LGA and LBM offer efficient and simple methods of simulating flow phenomena in complex geometries. They are ideal tools for parallel computers and as these methods become more sophisticated and realistic, more traditional numerical methods of simulating fluid flow in porous media and fractured rock, such as finite-difference methods, lose their competitive edge, and will be phased out in the future [11].

This chapter briefly reviews the theory of cellular automata as it is the basis of the lattice gas and lattice Boltzmann method. Then the theory of the lattice Boltzmann method will be given in detail. This chapter then will discuss the concept of synthetic fractures as the lattice Boltzmann method will be used in the two-dimensional synthetic fractures. Finally the chapter concludes with the theory of artificial neural networks.

2.2. Cellular Automata Theory

Cellular Automata (CA) are discrete dynamical systems whose behavior is completely specified in terms of local relations. They are the model of a spatially distributed model of N cells, each of which is in one of k states at time t. At time t+1, each cell updates its state following a set of rules [12]. In addition to this, the state of a cell at time t+1 generally depends on its own state and the state of the other neighboring cells at time t.

CA can also be defined as mathematical models for complex natural systems containing large numbers of simple identical components with local interactions [13]. Cellular Automata can be characterized as follows [14]:

- CA is regular arrangements of single cells of the same kind.
- Each cell holds a finite number of discrete states.
- The states are updated simultaneously at discrete time levels.
- The update rules are deterministic and uniform in space and time.
- The rules for the evolution of a cell depend only on a local neighborhood of cells around it.

CA is valuable because of its capability to display complex behavior by using the simple update rules. This property makes CA a strong candidate for the simulation tool for the physical phenomena like fluid flow. The single most successful practical application of CA as *computing* devices has been made thus performed in the field of fluid mechanics [15]. Despite still being in their infancy, CA models of fluid dynamics have already demonstrated that they can reproduce many of the essential features of thermodynamical and hydrodynamical behavior.

This capability of CA is proved and they stated that a simple cellular automata obeying nothing but conservation laws at microscopic level was able to reproduce the complexity of real fluid flows and named it as “Lattice Gas Automata (LGA)” [16]. Lattice gas automata belong to a special class of

cellular automata designed to study various physical systems. Lattice Boltzmann method, which is used in this thesis was developed in response to the drawbacks of the lattice gas automata method [17]. The main difference between two methods is that lattice Boltzmann method describes the particle density as a continuous function instead of a Boolean variable. This method reduces the statistical noise produced by the Boolean arithmetic of the lattice gas automata.

2.3. Lattice Boltzmann Method

Lattice Boltzmann method as all other CA based methods that simulate natural phenomena like fluid flow uses an approach that is different from the conventional methods. This approach is named as "*bottom-up*" approach and it is totally different from "finite-element" and "finite-difference" methods. Figure 2.1 shows the difference between two methods.

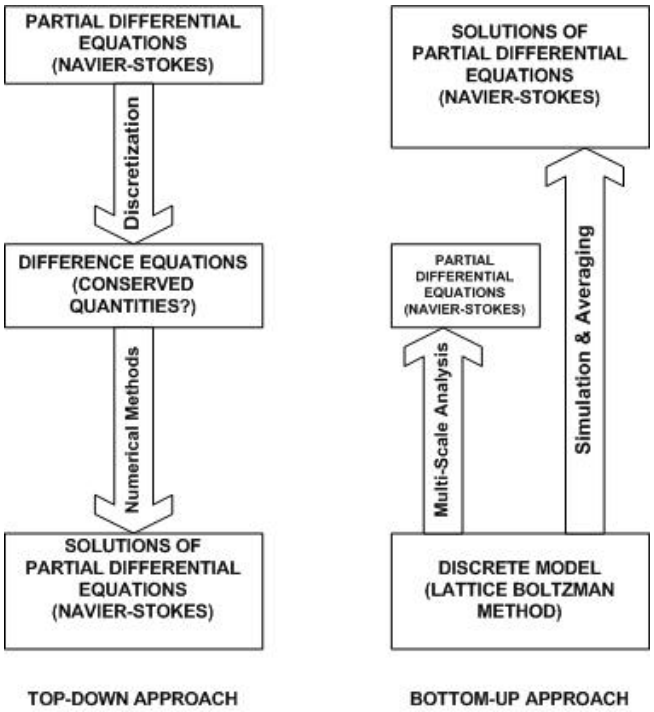

Figure 2.1. Difference between Top-Down and Bottom-Up Approach

In traditional methods (top-down approach) normally partial differential equations (PDEs) are used to simulate fluid flow. These PDEs are discretized by finite differences, finite volumes or finite elements. The resulting algebraic equations or systems of ordinary differential equations are solved by standard numerical methods. As for numerical simulations conventional Navier-Stokes codes are applied to flows in both porous and fractured media, but they have some drawbacks like long computation times, poor convergence and numerical instabilities.

Lattice Boltzmann method (LBM) which is a variant of "bottom-up" approach is developed as another computational method that is more efficient and use simple rules to represent the fluid flow rather than partial differential equations. LBM is a discrete computational method based upon the Boltzmann equation, it describes macroscopic fluid flow by the collective behavior of many fictitious molecules but not by full molecular dynamics, it is referred to as a mesoscopic description of microscopic physics [18]. This idea is illustrated in Figure 2.2.

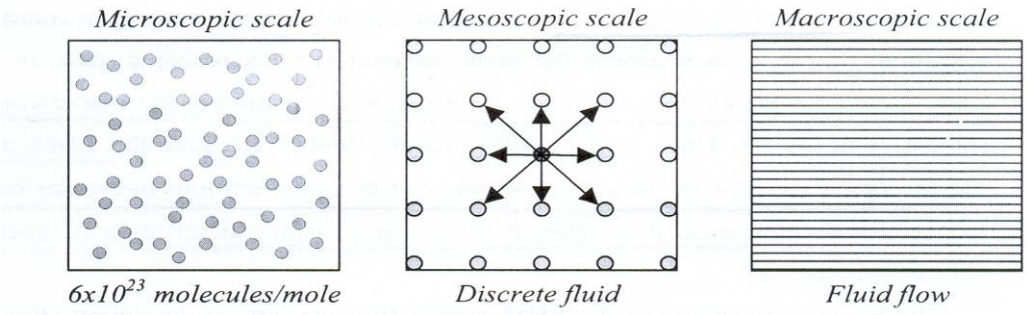

Figure 2.2. Schematic Description of the Lattice Boltzmann Method [18]

One of the most important advantages of the LBM is its capability for handling fluid flow especially in complex geometries [19]. The complex geometric details in the porous media and fractures can be handled in terms of

simple bounce-back rules and the method readily applied to any arbitrary discrete geometry.

2.3.1. Two-Dimensional Lattice Boltzmann BGK model

In our work two-dimensional Bhatnagar-Gross-Krook (BGK) Lattice Boltzmann method is used. This model uses a D2Q9 lattice with nine discrete velocities. Velocity vectors are illustrated in Figure 2.3.

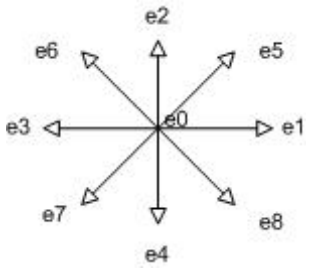

Figure 2.3. The Nine-Speed Square Lattice Velocity Vectors

The velocity directions of the D2Q9 Lattice Boltzmann BGK model are defined as [20].

$$e_k = \begin{cases} (0,0) & k=0 \\ (\cos[(k-1)\pi/2], \sin[(k-1)\pi/2]) & k=1,2,3,4 \\ \sqrt{2}(\cos[(k-5)\pi/2+\pi/4], \sin[(k-5)\pi/2+\pi/4]) & k=5,6,7,8 \end{cases} \quad (2.3.1)$$

Let $f_k(x,t)$ be a non-negative real number describing the distribution function of the fluid density at site x and time t moving with velocity e_k towards the neighboring lattice site located at $x+e_k$ where the subscript k refer to the velocity direction (k=1,…,9).

The distribution functions evolve according to the Boltzmann equation that is discrete in both time and space.

$$f_k(\mathrm{x} + c\mathrm{e}_\mathrm{k}\Delta t, t + \Delta t) = f_k(\mathrm{x}, t) + \Omega_k(\mathrm{x}, t) \qquad (2.3.2)$$

where $c = \Delta x/\Delta t$, Δx is the lattice grid spacing and Δt is the time step. The evolution of distribution function f_k is a two-step process; collision and propagation. In collision step, the mass and momentum are redistributed by the collision operator at each lattice node, and in propagation step, the updated distribution at location x streams to neighboring location $x + e_k$. Two-step process is repeated until the distribution reaches steady state.

$\Omega_k(x,t)$ is the collision operator representing the rate of change of the particle distributions due to collision [21] and is given by

$$\Omega_k(x,t) = -\frac{1}{\tau}[f_k(x,t) - f_k^{eq}(x,t)] \qquad (2.3.3)$$

where τ is the dimensionless single relaxation time that controls the rate of approach to equilibrium and f_k^{eq} is the equilibrium particle distribution function, which is determined by [20].

$$f_k^{eq}(\mathrm{x}, t) = w_k\rho + \rho s_k(\mathrm{u}(\mathrm{x}, t)) \qquad (2.3.4)$$

where

$$s_k(\mathrm{u}) = w_k\left[3\frac{(\mathrm{e_k}.\mathrm{u})}{c} + 4.5\frac{(\mathrm{e_k}.\mathrm{u})^2}{c^2} - 1.5\frac{|\mathrm{u}|^2}{c^2}\right] \qquad (2.3.5)$$

with weight coefficient

$$w_k = \begin{cases} \frac{4}{9} & k=0 \\ \frac{1}{9} & k=1,2,3,4 \\ \frac{1}{36} & k=5,6,7,8 \end{cases} \qquad (2.3.6)$$

Collection of particles of unit mass and unit momentum moves on the lattice. Mass and momentum of the particles are locally conserved after collision of the particles.

The fluid density ρ and velocity u are obtained from the density distribution function $f_k(x,t)$:

$$\rho = \sum_k f_k \qquad (2.3.7)$$

$$\rho \mathrm{u} = \sum_k c e_k f_k \qquad (2.3.8)$$

At macroscopic scale the behavior of these particles is the same as that is predicted by the incompressible Navier-Stokes equations [14].

2.3.1.1. Algorithm for the Lattice Boltzmann Application

There are many different algorithms available for putting the lattice Boltzmann method into computational code. The following pseudo code shows the how LBM was implemented in this study.

Start Program
Read in Obstacle Location File
Set initial density distribution
Loop for T time Steps
{
    Redistribute along first lattice column
    Propagate fluid particles
    Check for obstacle (bounce-back)
    Calculate density and velocity with Equations 2.3.7 & 2.3.8
    Calculate permeability
    If((perm-oldperm)<tolerance_value))
    exit loop
}
Write velocity data to file
End

2.3.1.2. Boundary Conditions

A boundary condition with a constant pressure difference is used at inlet and outlet of the fracture aperture, where all fluid densities are propagated from non-occupied nodes along the lattice-connection lines to their next neighbors.

The physical boundary condition at solid-fluid interfaces is the no-slip boundary condition, which in LBM is usually realized as bounce-back rule. This is physically appropriate whenever the solid wall has a sufficient rugosity to prevent any net fluid motion at the wall [6]. The complete bounce-back scheme is used to simulate the no-slip boundary condition, which requires that when a particle distribution streams to a solid boundary node, it scatters back to the node it came from. The velocity vector of all fluid densities is inverted, so

all the fluid densities will be sent back to the node where they were located before the last propagation step, but with opposite velocity vector.

2.4. Synthetic Fractures

The geometry of the fracture surfaces affects the hydraulic properties of the fractured rock. Roughness at the surface of the fractures could be described efficiently by using the fractal geometry concepts [22]. Since studying rough, anisotropic fractures in the laboratory is difficult, instead synthetic fractures could be used. Synthetic fracture is the term used to describe fractures that are created numerically in such a way that they share the same mean geometrical characteristics as specific natural fractures measured by profiling, by a process known as tuning [23]. For example numerical synthetic fractures can be created from unmatched fractal surfaces [24]. Geostatistical techniques like conventional kriging and conditional simulation [25] could also be used to create synthetic fractures. In this work numerical modeling is used to simulate fluid flow in synthetic rock fractures that share the same physical properties with the natural fractures. In this thesis SynFrac software is used to create synthetic fractures [23]. This software uses modified methods for producing synthetic rough surfaces whose geometric properties are tuned to mimic natural fractal surfaces in rocks in order to create synthetic fractures that are statistically identical to those found in rocks.

2.5. Artificial Neural Networks

Neural computing is an alternative to programmed computing which is a mathematical model inspired by biological models [26]. This computing system is made up of a number of artificial neurons and a huge number of interconnections between them. According to the structure of the connections, two different classes of network architectures could be identified: layered feed-

forward neural network and non-layered recurrent neural network. Figure 2.4 shows the layered feed-forward neural network.

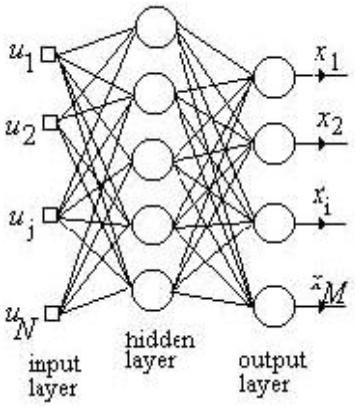

Figure 2.4. Layered Feed-Forward Neural Network

In layered feed-forward neural networks, the neurons are organized in the form of layers. The leftmost layer is called the input layer and it is made up of special input neurons, transmitting only the applied external input to their outputs. The neurons in a layer get input from the previous layer and feed their output to the next layer, but connections to the neurons in the same or previous layers are not permitted. The last layer of neurons is called the output layer and the layers between the input and output layers are called the hidden layers. In single layer networks there is only the layer of input nodes and a single layer of neurons constituting the output layer. If there are one or more hidden layers, such networks are called multilayer networks. The lines represent weighted connections (i.e., a scaling factor) between processing elements.

Supervised and unsupervised are the approaches to train the Artificial Neural Network (ANN). Supervised training involves a mechanism of providing the network with the desired output either by manually "grading" the network's performance or by providing the desired outputs with the inputs. Unsupervised training is where the network has to make sense of the inputs

without outside help. After the input pattern was presented to the network and processed by all layers, errors (the difference between what we want and what we got) that can be used to adjust the network. An algorithm called back-propagation [27] is used to adjust the weights a small amount at a time in a way that reduces the error. The network is trained by repeating this process many times. The goal of the training is to reach an optimal solution based on the performance measurement.

CHAPTER 3

STATEMENT OF THE PROBLEM

The main aim of this thesis is to simulate the single phase fluid flow and calculate absolute permeability in two-dimensional fracture apertures. These fracture apertures are created synthetically, and they represent the physical properties of actual rock fractures. This thesis also focuses the relationships between the fracture parameters like fractal dimension, anisotropy factor or mismatch length and the absolute permeability of the fractures.

Permeability values in porous and fractured medium could be calculated with many methods. These methods could be empirical relations or numerical techniques. In this study, a novel numerical technique named as "Lattice Boltzmann Automaton Model" is used. Three-dimensional synthetic fractures are created by SynFrac software; two-dimensional slices are obtained from these fractures and converted into binary format in order to use as an input for the lattice Boltzmann simulations. Outputs of these simulations are used to calculate absolute permeability values. Numerous simulation runs are performed and artificial neural networks (ANN's) are used to obtain a relationship between the fracture parameters and calculated absolute permeability values. ANN results are also analyzed to determine the fracture parameter that affects the absolute permeability mostly.

CHAPTER 4

METHODOLOGY

4.1. Introduction

In laboratory experiments, two consecutive steps exist; firstly the experimental setup is formed, then the experiment is performed. The main purpose of the experiments is to observe the changes in the results by the modifications in the inputs of the experimental setup. The work that is done in this thesis could be considered as a "Virtual Rock Physics Laboratory". Virtual experiments are performed in numerically created synthetic core samples by simulating the fluid flow.

The consecutive steps in this work could be defined as; synthetic fracture generation with SynFrac software, post-processing synthetic fracture data to make it suitable for the simulation, running the lattice Boltzmann simulation, calculating the absolute permeability values and training the artificial neural network with the simulation results. The details of these steps will be defined in the following sections.

4.2. Synthetic Fracture Generation by SynFrac

SynFrac software originally generates three-dimensional fractures. The resolution of the fracture can be altered with in the range from 64x64 to 1024x1024. In addition to this, various parameters like fractal dimension or

anisotropy factor could be altered to generate fractures that have the same resolution but different physical properties. Fractal dimension for each surface is a value between 2 and 3; this value determines the roughness of the fracture surface. Another parameter that is altered is the anisotropy factor, which is used to generate anisotropic synthetic fractures. Anisotropy factor is chosen between 1 and 3. Difference of this value from unity means that all the scales in one direction along the fracture surface will be greater than the scales in other direction.

With the parameters given, SynFrac software creates two fracture surfaces, which form a three-dimensional fracture aperture as illustrated in Figure 4.1.

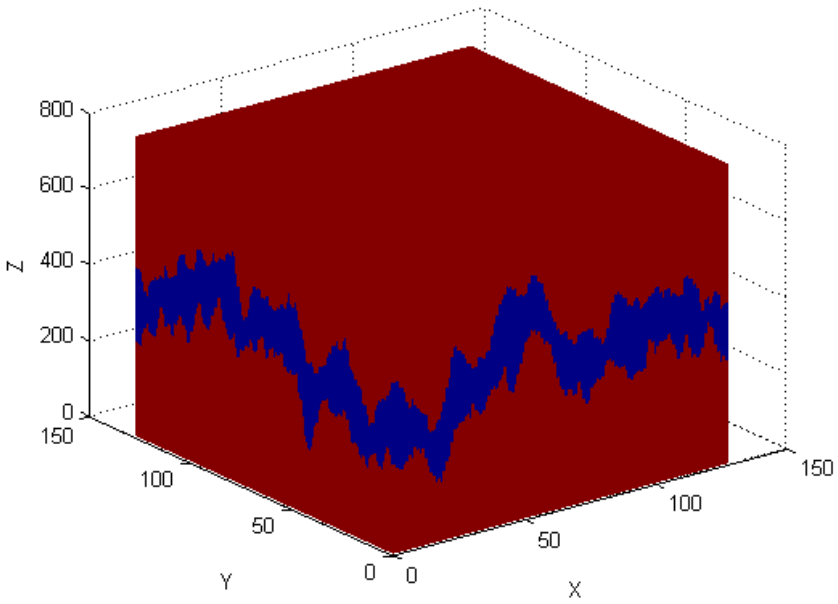

Figure 4.1. Three-Dimensional Fracture Aperture Created by SynFrac.

As the lattice Boltzmann simulation is performed at two-dimensions in this study, two-dimensional slices are obtained from the three-dimensional

fracture apertures. Figure 4.2 shows a two-dimensional fracture aperture obtained by slicing the three-dimensional fracture for a given plane.

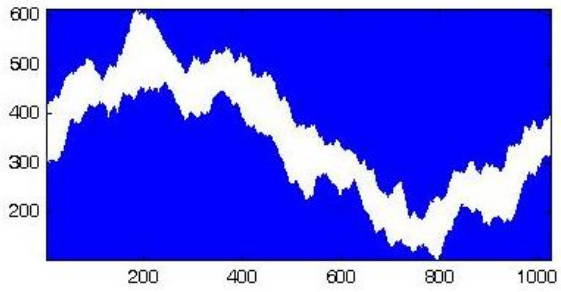

Figure 4.2. Two Dimensional Fracture Aperture Obtained by Slicing.

This sliced two-dimensional fracture forms the basis for our lattice Boltzmann simulation. SynFrac software outputs the heights of the top and bottom surfaces of the created fracture; output data is shown in Table 4.1.

Table 4.1. Fracture Data Obtained from SynFrac.

X-Loc	Y-Loc	Top(mm)	Bottom(mm)	Aperture(mm)
1	1	4.879	4.140	0.739
1	2	4.852	4.151	0.701
1	3	4.848	4.165	0.683
1	4	4.856	4.165	0.691
⋮	⋮	⋮	⋮	⋮
800	1023	4.847	4.162	0.685
800	1024	4.831	4.142	0.689
⋮	⋮	⋮	⋮	⋮
1024	1021	4.879	4.142	0.737
1024	1022	4.868	4.154	0.714
1024	1023	4.877	4.159	0.718
1024	1024	4.882	4.152	0.730

This data must be digitized that means it should be converted into binary format (1's and 0's) in order to be used with lattice Boltzmann algorithm. This idea is illustrated in Figure 4.3, where 1's represent grains and

0's represent pore space. A two-dimensional array data structure named as *pore[x] [y]* contains the information about the synthetic fracture, where x and y is the size of the lattice grid. This array is in binary format and porosity of the fracture could be calculated by the Equation 4.2.1.

$$image\_porosity = 1 - mean(pore[x][y]) \qquad (4.2.1)$$

As that porosity values are not real fracture porosities, this new definition of porosity in our study is named as *image porosity.* Calculated image porosity values for each fracture aperture are tabulated in Appendix A.

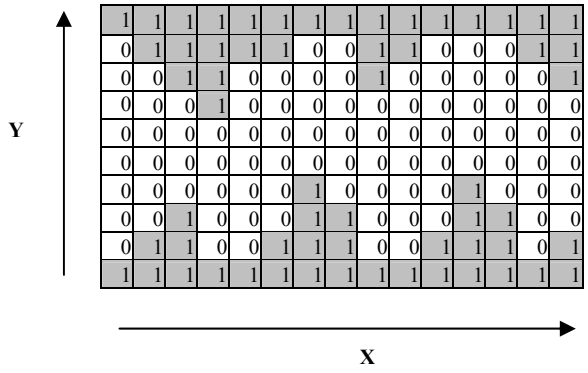

Figure 4.3. Binary Representation of Two-Dimensional Fracture Aperture.

In order to increase accuracy of the simulation synthetic fractures are created at maximum resolution of SynFrac (1024x1024). After slicing two-dimensional fractures from the original fracture that is created by SynFrac a fracture aperture as in Figure 4.2 is obtained. This fracture aperture is represented in binary format as in Figure 4.3. with 2D resolution of, 1024 in x-direction and a value which is determined according to the minimum value of the bottom surface and maximum value of top surface, this value in y-direction changes between 500 and 700.

4.3. Lattice Boltzmann Simulation of Fluid Flow

Two-dimensional single-phase lattice Boltzmann simulation runs are performed in order to understand the effects of the parameters that are altered during the fracture generation phase to the absolute permeability of the fractures. At each step synthesized fracture with its fractal dimension or anisotropy factor altered converted into binary format and used as an input for the lattice Boltzmann simulation, other parameters are held constant as in Table 4.2. Velocity vectors on each grid point are calculated by the lattice Boltzmann method.

Absolute permeability k of the fracture could then be obtained by calculating the mean flux from the velocity vectors and with the Darcy's law. First the mean flux is calculated by the Equation 4.3.1, where n_x and n_y is the size of the lattice.

$$\bar{q} = \frac{\sum q}{n_x * n_y} \tag{4.3.1}$$

Then permeability k could be calculated by Equation 4.3.2.

$$\bar{q} = \frac{k}{\mu}\frac{dP}{dx} \tag{4.3.2}$$

Where μ is the dynamic viscosity of the fluid, $\bar{q}$ is the volumetric fluid flux through the fracture, it is calculated by velocity averaged over all lattice nodes in the pore space, and dP is the constant pressure gradient, which is equal to 1 atm.

Table 4.2. Constant Parameters used in the Lattice Boltzmann Method Simulations

Resolution	1024
Physical size (mm)	100.00
Mismatch length (mm)	15.00
Transition length (mm)	10.00
Standard deviation (mm)	1.00
Max matching fraction	1.00
Min matching fraction	0.00

The model of capillary tubes is used to verify that our lattice Boltzmann implementation is successful.

Poiseuille's equation for fluid conductivity of capillary tubes is given as.

$$Q = \frac{\pi r^4 \Delta P}{8 \mu L} \tag{4.3.3}$$

where μ is the dynamic viscosity, r is the radius of the tube, ΔP is the pressure difference and L is the length of the tube.

From Darcy's law it is also known that

$$Q = Ak \frac{\Delta P}{L \mu} \tag{4.3.4}$$

Equating Darcy's law and Poiseuille's equations for fluid flow in a tube gives:

$$k = \frac{r^2}{8} \tag{4.3.5}$$

where k is the permeability, if r is in centimeters and k is in darcys it is given by [18].

$$k = 12.50x10^{6} r^{2} \tag{4.3.6}$$

In order to verify the exactness of our lattice Boltzmann implementation, the permeability values calculated by Equation. 4.3.5 are compared by the permeability values obtained by the lattice Boltzmann method. Table 4.3 presents the results of the verification.

Table 4.3. Lattice Boltzmann Method in Pipe Flow

	LBM (md)	**Analytic (md)**
Case 1 (31x101)	$2.81505x10^{6}$	$2.8125x10^{6}$
Case 2 (101x251)	$3.16715x10^{7}$	$3.125x10^{7}$

4.4 Training Artificial Neural Networks with Simulation Data

Feed-forward neural network with two hidden layers is trained with the data of the lattice Boltzmann simulations, which are performed by altering the anisotropy factor and fractal dimension.

In our simulations the values of the anisotropy factor varied between 1.0 - 3.0 and fractal dimension values are between 2.21 - 2.50. Values in Table 4.2 are held constant and they are not used for training the Artificial Neural Network. Figure 4.4 shows the architecture of our system.

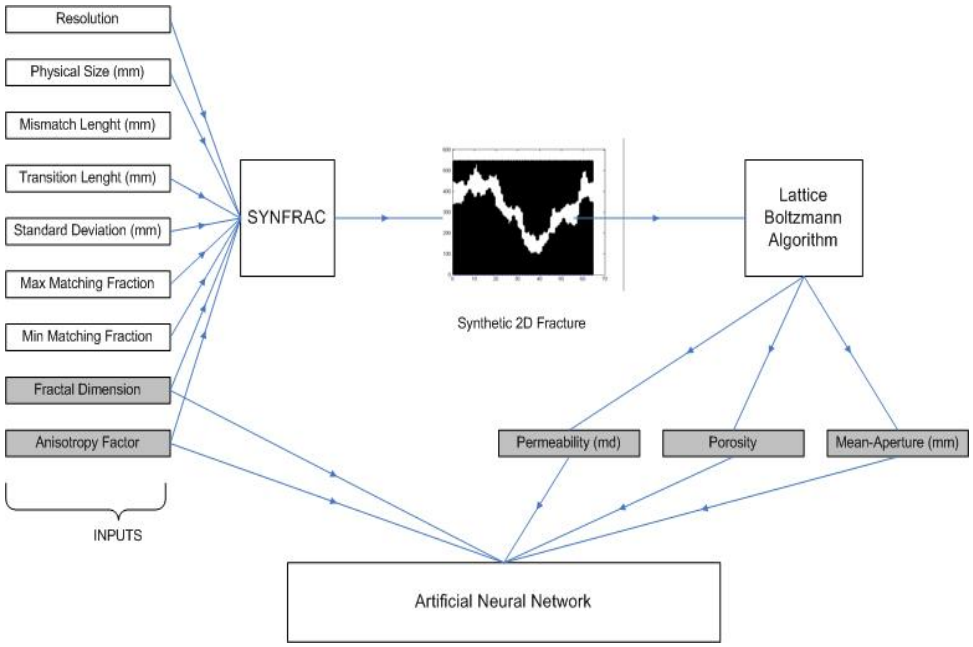

Figure 4.4. Architecture for the LBM Simulation and ANN Training.

According to the Figure 4.4 fractal dimension, anisotropy factor, porosity, mean aperture and permeability is used to train the ANN, among these parameters some of them are chosen as input parameters and some of them are chosen as output parameters. As our aim in this work is to determine the effect of change in fracture parameters to the permeability, the calculated permeability values from the LBM simulations are selected as output parameter and fracture parameters as fractal dimension, anisotropy factor, mean aperture and porosity are selected as input parameters, this relationship is shown in Figure 4.5.

Since there were several orders of magnitude difference between the input data the LBM permeability was scaled to values between 0 and 1 by dividing the LBM permeabilities to maximum calculated permeability value.

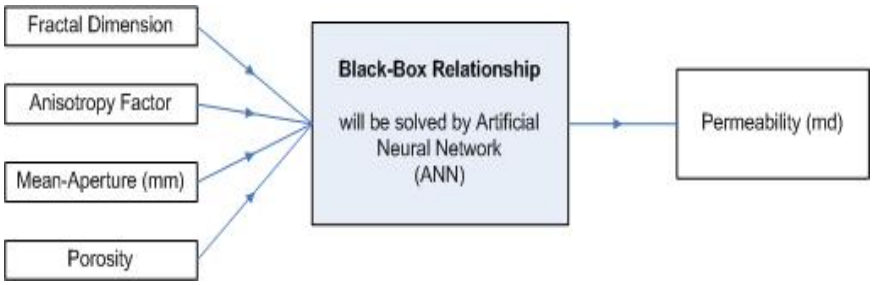

Figure 4.5. Input and Output Parameters for ANN.

During the training process for determining the weights, randomly selected 10% of data was kept for later verification of network accuracy. These data are often referred to as test or validation data. Once the weights have been determined through back propagation the test data were used as network inputs for determining the network's accuracy in predicting unprocessed data sets. The quality or goodness of training was judged based on the closeness of the prediction of the remaining "testing" data. In order to quantify the model performance a mean square error (MSE) value was used.

CHAPTER 5

RESULTS AND DISCUSSION

Several lattice Boltzmann simulation runs were conducted to understand the relation between the altered fracture parameters and the absolute permeability. This chapter presents all the results of the lattice Boltzmann simulations and the relations that are obtained both by numerical methods and ANN's.

5.1. Effect of Fracture Geometry to Flow Patterns.

By using the velocity vectors calculated by the LBM, regions of high velocity and low velocity flow were identified. Several runs were conducted to identify flow velocity patterns. In order to isolate the effect of location selection while slicing the two-dimensional planes from the three-dimensional fracture, synthetic fractures were selected from the same location in 3D. That's why the fracture geometry was similar but the rugosity was somewhat different for each case. As it can be seen from the Figure 5.1 and Figure 5.2, the fracture sloped upwards first then following a downhill that ended with increasing slope. Each figure shows the effect of altered fracture parameter (fractal dimension and anisotropy factor) to the fracture geometry and flow patterns. The values in the axes indicate the number of grid points that is used to represent the fracture aperture. Figures contain the fracture apertures created for the minimum and maximum values of the fractal dimension and anisotropy factor.

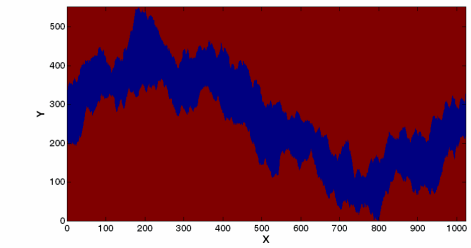

Fractal Dimension: 2.21
Anisotropy Factor: 1.0

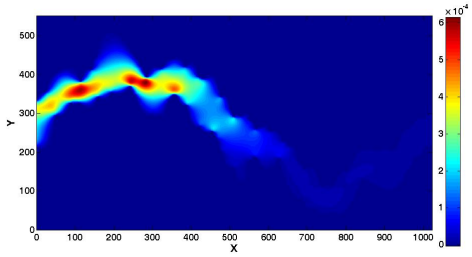

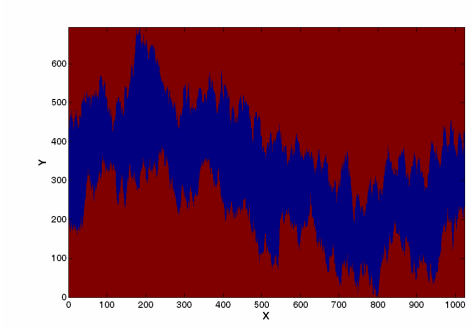

Fractal Dimension: 2.50
Anisotropy Factor: 1.0

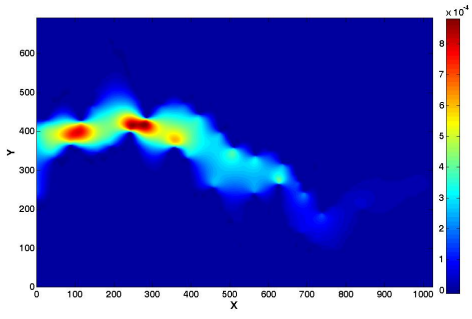

Figure 5.1. Effect of Fractal Dimension to Fracture Geometry and Velocity Distribution

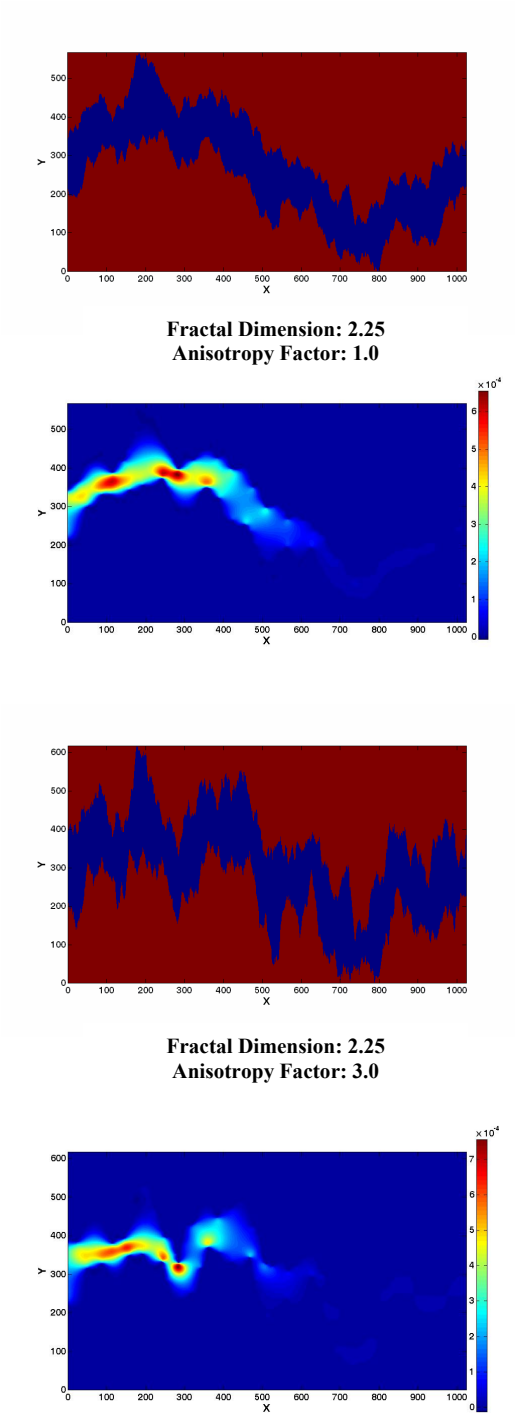

Figure 5.2. Effect of Anisotropy Factor to Fracture Geometry and Velocity Distribution

From the figures above it could be observed that for a constant pressure gradient the highest velocity was observed near the inlet of the fracture corresponding to locations where the aperture was significantly lower than the rest of the fracture. These locations are shown with arrows in Figure 5.3.

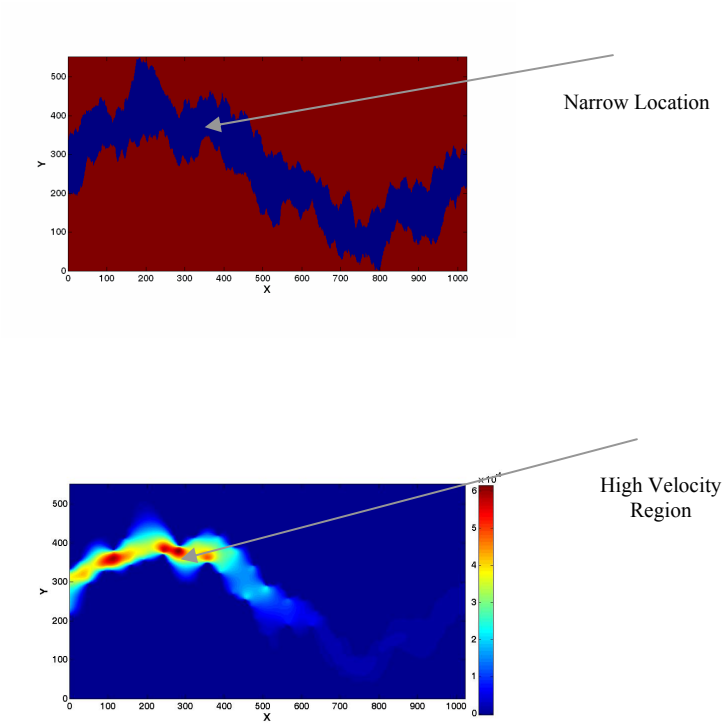

Figure 5.3. Low and High Velocity Regions

From the Figure 5.3 it could be seen that the high velocity flow dissipated near the end of the fracture. This observation is valid also for the other cases in Figure 5.1 and Figure 5.2.

As the fractal dimension increased (from 2.21 to 2.5 corresponding to %13 increase), the magnitude of the highest velocity observed increased (approximately %30). On the other hand, as the anisotropy factor increased from 1 to 3, the location of highest velocities along the fracture changed. Moreover, the magnitude of the highest velocity decreased.

5.2. Fractal Dimension Permeability Relationships

Lattice Boltzmann simulations were conducted to understand the effect of fractal dimension to fracture permeability. Several runs are performed by changing the fracture dimension between the values 2.21 and 2.50 and all other parameters are held constant. Table 5.1 presents the results of these simulations with the calculated lattice Boltzmann permeability values.

Table 5.1. Results of the Lattice Boltzmann Simulations for Different Fractal Dimensions

Fractal Dim	**Mean-Aper, h (cm)**	**Cubic Law Perm (md)**	**LB-Perm (md)**	**Exponent β**	h^{β}
2,21	0,13443	1,5255355E+08	1,591330E+06	4,273842	0,000189
2,25	0,1455	1,7871290E+08	1,682210E+06	4,420483	0,000199
2,30	0,16051	2,1748740E+08	1,811020E+06	4,61739	0,000215
2,32	0,16691	2,3517688E+08	1,861850E+06	4,702768	0,000221
2,35	0,17693	2,6426088E+08	1,941310E+06	4,836935	0,00023
2,38	0,18746	2,9665190E+08	2,016380E+06	4,981296	0,000239
2,40	0,19478	3,2027175E+08	2,053540E+06	5,086773	0,000243
2,45	0,21411	3,8699363E+08	2,182700E+06	5,359477	0,000259
2,47	0,22224	4,1694078E+08	2,232300E+06	5,477341	0,000264
2,50	0,23486	4,6563758E+08	2,294030E+06	5,667327	0,000272

Figure 5.4 shows permeability values that are calculated by LBM vs. mean aperture – fractal dimension ratio. The fracture permeability increases linearly with a high correlation coefficient as the mean aperture fractal dimension ratio increases.

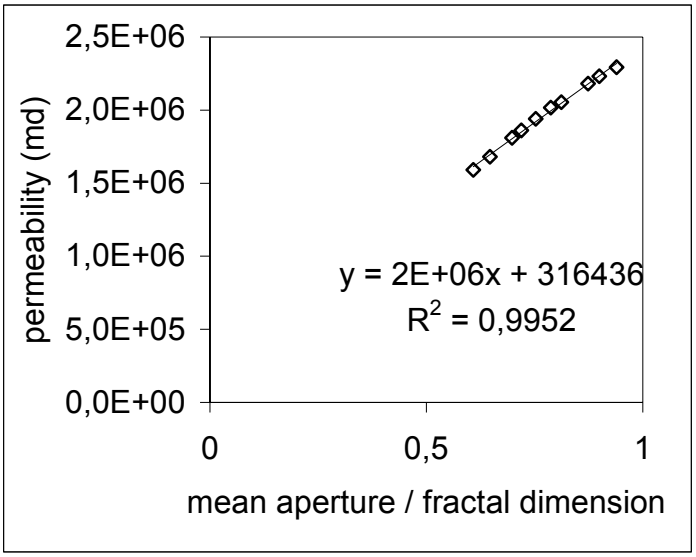

Figure 5.4. Relationship between LBM Permeability and Mean Aperture-Fractal Dimension Ratio.

LBM fracture permeabilities were two orders of magnitude lower than the permeabilities obtained from the cubic law [1].

$$k = 84.4x10^5 h^2 \tag{5.2.1}$$

where h is the mean aperture in centimeters and k is in darcys. This suggests that for a rough self-affine fracture one may have a fractal dimension dependent power that is larger than 2. Our simulations suggest an exponent range from 4.27 to 5.66 that are in accordance with the range (2 to 6) provided by Zhang, X et al. [28].

Permeability could be estimated from the Equation 5.2.2, where δ is mean aperture and β is the exponent [28].

$$k \approx \delta^{\beta} \tag{5.2.2}$$

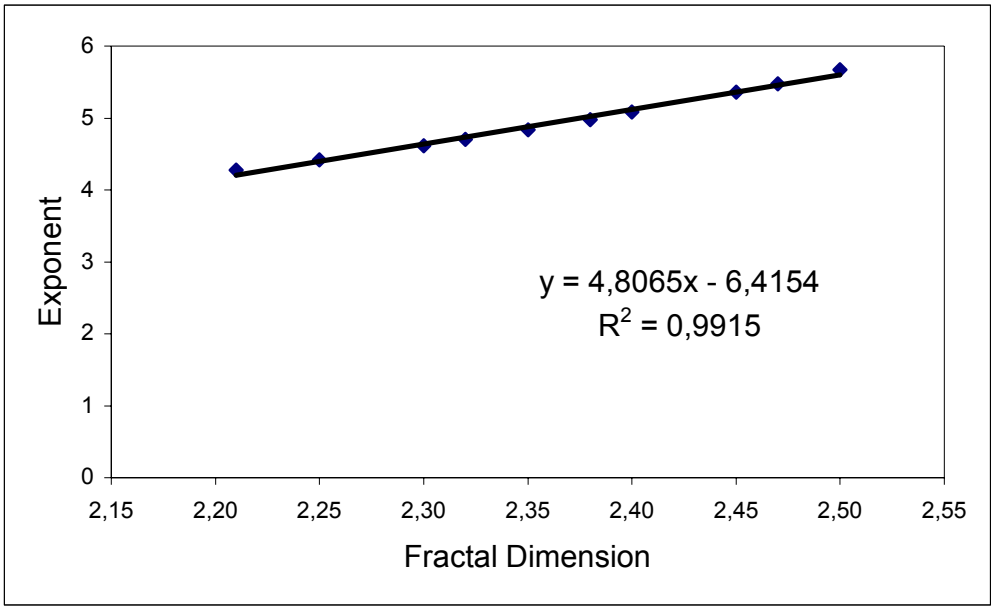

Figure 5.5. Relationship between the Exponent β and Fractal Dimension

Moreover, for anisotropy equal to 1 it was observed that there is a linear relationship between the fractal dimension D and the exponent β, which is shown in Figure 5.5.

Exponent β is given by the Equation 5.2.3.

$$\beta = 4.8065D - 6.4154 \tag{5.2.3}$$

Equation 5.2.4, which is the modified version of the Equation. 5.2.1 and Equation 5.2.3 could be used to calculate the permeability values of the fractures, by entering the mean aperture h and fractal dimension D as an input.

$$k = 84.4x10^5 h^{\beta} \tag{5.2.4}$$

5.3. Anisotropy Factor Permeability Relationships

Another set of simulations was performed to understand the effect of the changes in anisotropy factor to the fracture permeability. Several runs are performed by changing the anisotropy factor between the values 1.0 and 3.0 and all other parameters are held constant. Table 5.2 presents the results of these simulations for the fractal dimension of 2.25 with the calculated lattice Boltzmann permeability values.

Table 5.2. Permeability Values of the Fractures for Different Anisotropy Factors

Anisotropy Factor	**Mean-Aper,h (cm)**	**LB-Permeability (md)**	**Exponent β**	h^{β}
1,00	0,14550	1,68E+06	4,420463	0,000199
1,20	0,14777	1,60E+06	4,482942	0,000189
1,30	0,14925	1,56E+06	4,517993	0,000185
1,35	0,15005	1,53E+06	4,541212	0,000182
1,40	0,15088	1,51E+06	4,562485	0,000179
1,50	0,15262	1,46E+06	4,606695	0,000173
1,60	0,15444	1,42E+06	4,653111	0,000168
1,80	0,15825	1,33E+06	4,747482	0,000158
2,50	0,17860	1,21E+06	5,137125	0,000143
3,00	0,19238	1,15E+06	5,402273	0,000136

Similar results are reported in the literature for self-affine fractures [29], where permeability decreases with the increasing anisotropy. When

permeability values are plotted against anisotropy factors a second-order polynomial relationship was observed.

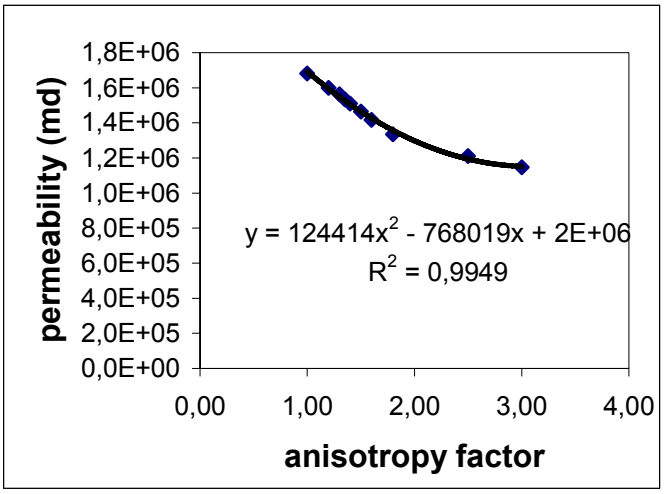

Figure 5.6. Relationship Between LBM Permeability and Anisotropy Factor.

It was observed that for a given fractal dimension, anisotropy and exponent relationship is linear. For example for D equals to 2.25 the following relationship was observed, where A is the anisotropy factor and β is the exponent.

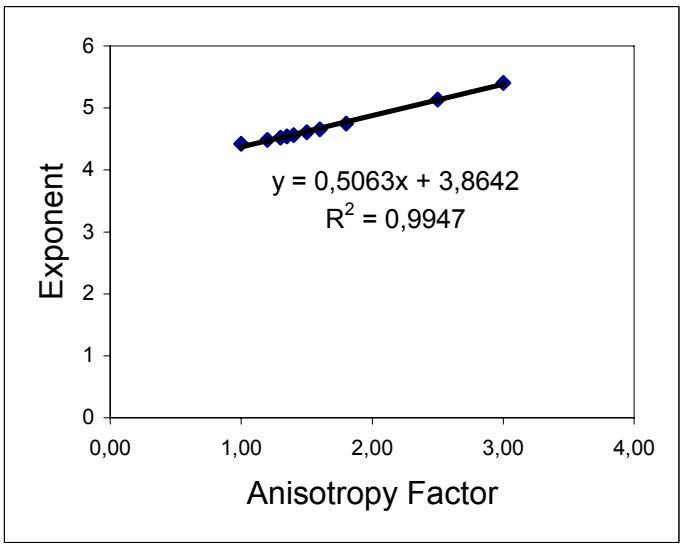

Figure 5.7. Relationship between the Exponent β and Anisotropy Factor

Exponent β is given by the Equation 5.3.1.

$$\beta = 0.5063A + 3.8642 \tag{5.3.1}$$

Again after calculating the exponent β with the equation above, permeability values could be calculated by using the Equation 5.2.4 for a given anisotropy factor and mean aperture.

As anisotropy factor increases, the exponent β increases with linear relationship and according to Equation 5.2.4 it is expected that permeability should increase with increasing anisotropy factor, but according to our simulation results permeability decreases with increasing anisotropy factor.

According to the Equation 5.2.4 permeability values depend not only to the exponent β, they also depend to the mean aperture h of the fracture, because of this reason permeability values change with the combination of the parameters h and β so, permeability values in Table 5.1 and Table 5.2 is consistent with h^{β} values that are presented in the last column of the tables.

5.4. Effect of Mismatch Length to Permeability and Flow Patterns

Another parameter that is altered is the mismatch length; it was previously shown that natural fractures are correlated to some degree at long wavelengths but at short wavelengths they are not identical [30]. These two different behaviors are modeled by a critical wavelength called the mismatch length. Above this length the fracture surfaces are correlated but below it the fractures behave independently. Figures 5.8, 5.9 and 5.10 show the effect of the change in the mismatch length both to the fracture geometry and flow patterns.

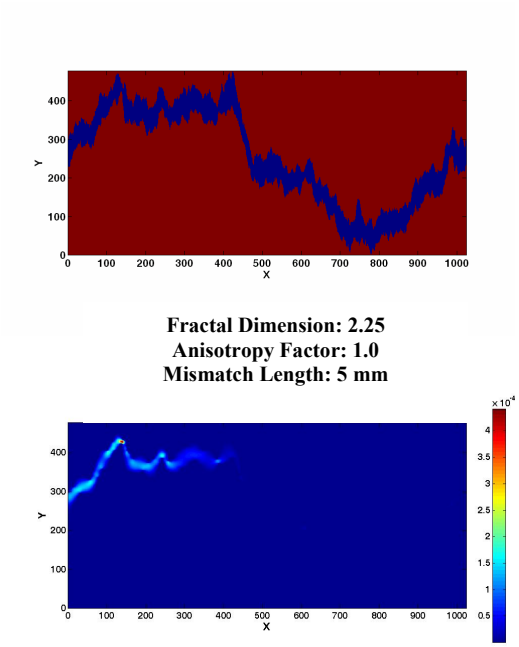

Figure 5.8. Generated Fracture Aperture and Velocity Distribution for Mismatch length of 5 mm.

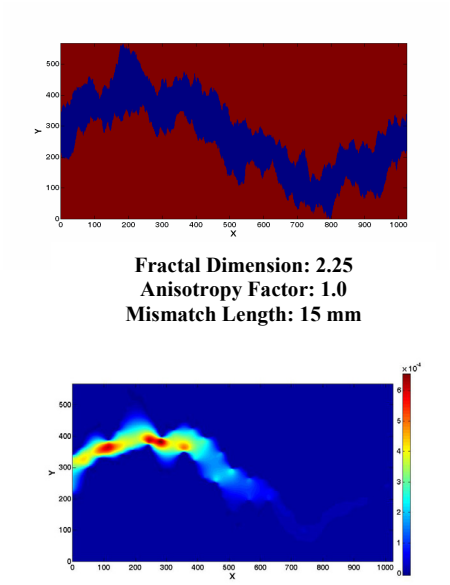

Figure 5.9. Generated Fracture Aperture and Velocity Distribution for Mismatch length of 15 mm.

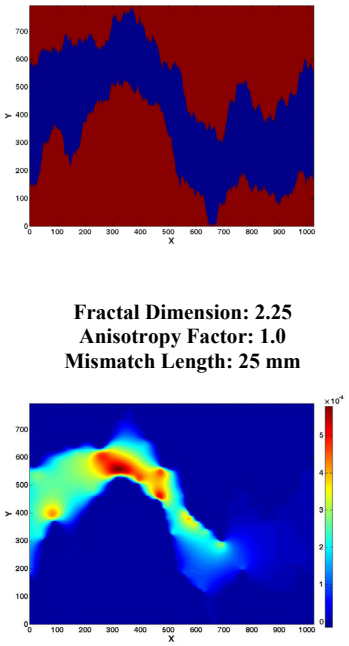

Figure 5.10. Generated Fracture Aperture and Velocity Distribution for Mismatch length of 25 mm.

As the mismatch length increased mean fracture aperture increased, this will affect the permeability values. The fracture became smoother for a given fractal dimension. This results in an increase in permeability. A linear relationship was observed with mismatch length and the LBM permeability and presented in Figure 5.11.

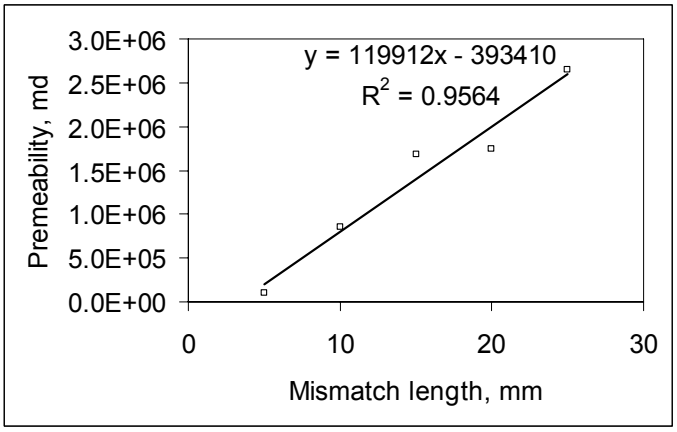

Figure 5.11. Relationship between LBM Permeability and Mismatch Length.

Relations obtained between the fracture parameters and permeability values seems consistent with the theoretical foundations and proposes some modifications to these rules, but a more detailed analyses should be performed with more simulation runs.

5.5 Artificial Neural Network Analysis of Simulation Data

In the previous sections, in each set ten simulations are performed to understand the effect of fractal dimension and anisotropy. In order to understand the effects of other parameters to permeability and to perform more detailed analyses of the previously examined parameters a sophisticated method must be used. New simulation runs are done and these data are used the train an Artificial Neural Network (ANN). This section presents the ANN analysis of the new lattice Boltzmann simulation results. The results of the simulations performed for new fractal dimensions and anisotropy factors are presented in Appendix A.

Permeability values obtained from the lattice Boltzmann simulation should be scaled, before using them to train ANN. It was observed that scaling permeability values decreases the mean square error significantly. These values are scaled between 0.40 and 1.0. Among these parameters lattice Boltzmann permeability is selected as output parameter and the others are selected as input parameters. This indicates that permeability of the fracture is related with fracture dimension, anisotropy factor, mean aperture and porosity. ANN will find how they are related to each other or in other words the change in which parameter affects the permeability most. Back propagation technique and 71 different LBM simulations were used to train different artificial neural networks and the best performing network was selected. The properties of the ANN model are presented in Table 5.3.

Table 5.3. ANN Model Properties

Input nodes	4
Output nodes	1
Hidden layer 1	20
Hidden layer 2	8
Momentum factor	0.1
Learning parameter	0.2

After training the ANN and reaching a small mean square error, trained ANN could be used to find relationships between the various fracture parameters and permeability. As the mean square error for the verification phase of the model is less than %0.1 (Figure 5.12) the results of the ANN are dependable.

In Figure 5.12 the mean square error for the training and validation phases of a dual layer ANN trained with the lattice Boltzmann simulation data is presented. The following figures are plotted by using the predictions of the ANN for different parameters.

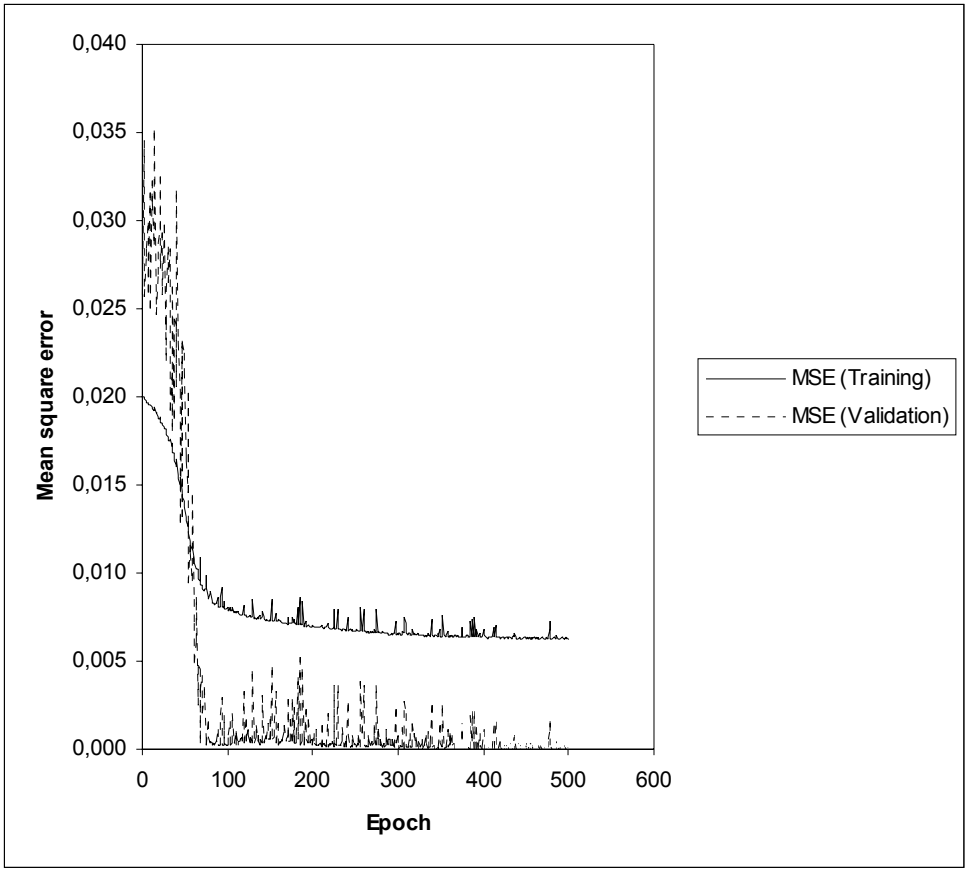

Figure 5.12. Mean Square Error for Training and Validation.

The mean square error value is closely to zero for validation phase of the ANN with two hidden layers. This indicates the success of the ANN model selected and the applicability of the model for future permeability predictions.

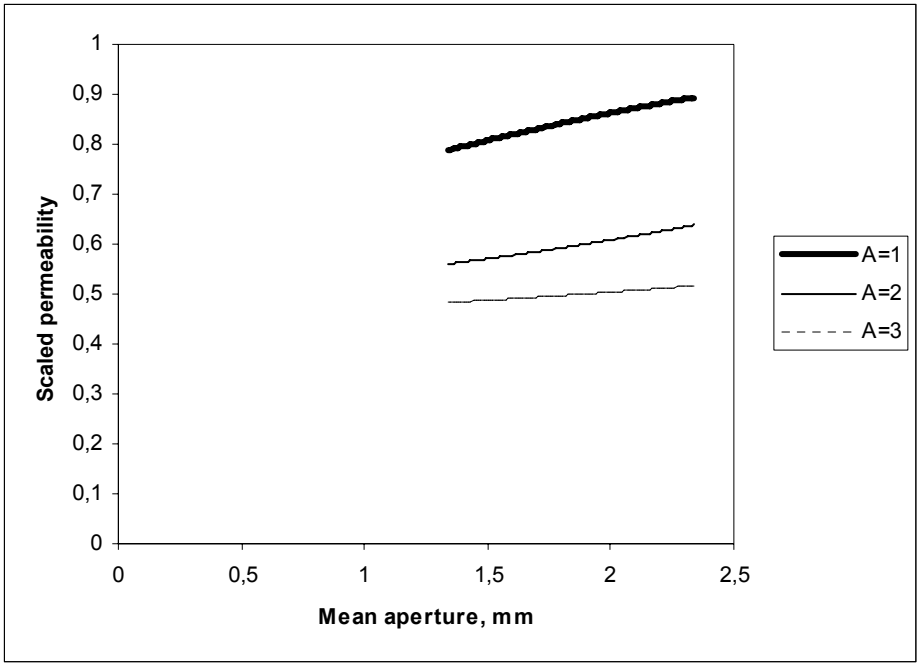

Figure 5.13. ANN Prediction for Mean Aperture, Anisotropy Factor and Permeability Relationship

Linear relationship exists between the mean aperture and permeability values, also the permeability values decreases with the increasing anisotropy factors. The strong effect of anisotropy factor to the permeability could be easily seen in Figure 5.13.

Another relationship is between the anisotropy factor and the permeability values. Previously in Figure 5.6 it was shown that second order polynomial relationship exists between permeability and anisotropy factor. This idea is also verified by the ANN outputs (Figure 5.14).

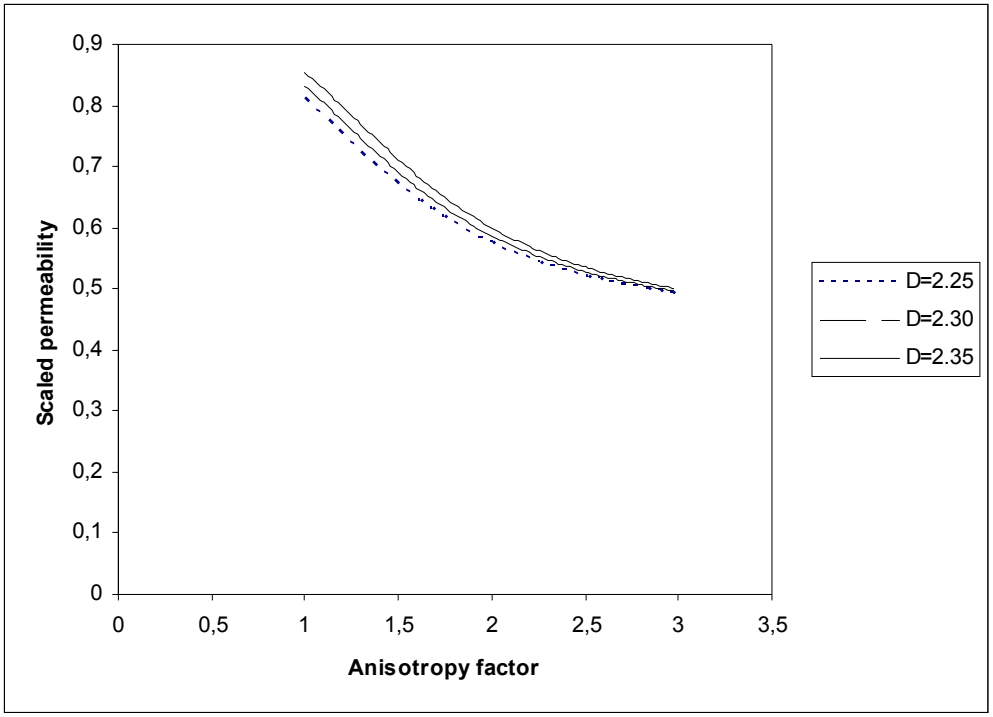

Figure 5.14. ANN Prediction for Fractal Dimension, Anisotropy Factor and Permeability Relationship

The results presented above are consistent with our previous predictions, the strong effect of anisotropy factor to the fracture permeability. It can be seen from the figure that the effect of fractal dimension to the permeability disappears after anisotropy value exceeds 2.5.

This strong effect could also be understood form Figure 5.15, that when the anisotropy value reached 3.0, the effect of fracture dimension to the permeability becomes so negligible.

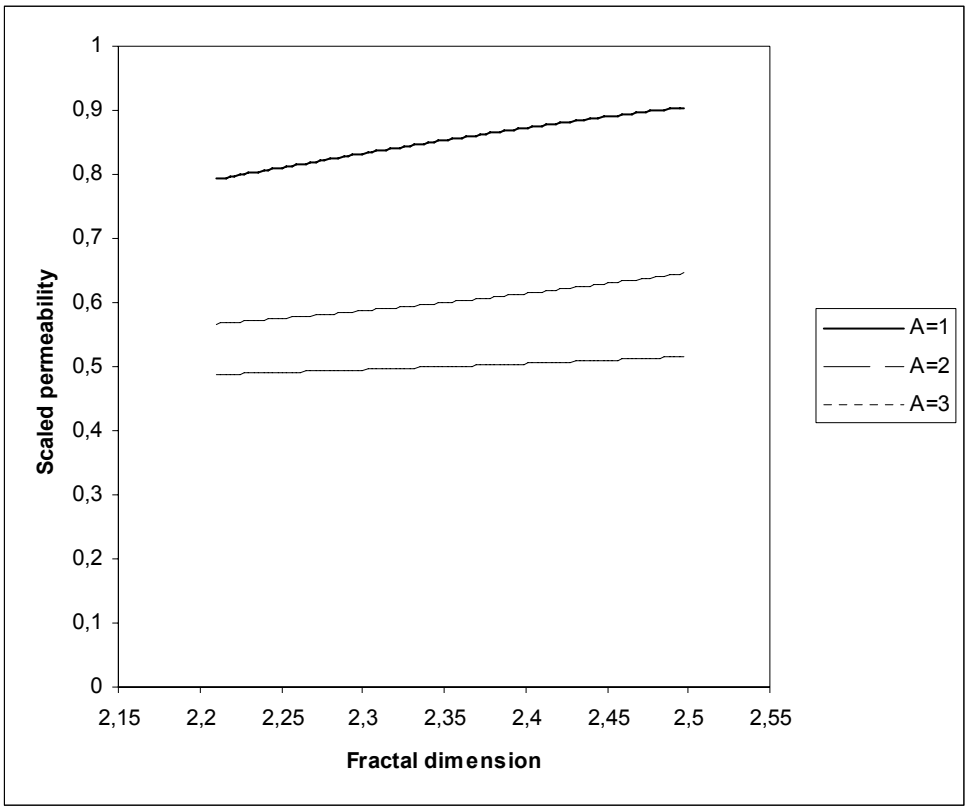

Figure 5.15. ANN Prediction for Anisotropy Factor, Fractal Dimension, and Permeability Relationship

Usage of ANN's is very useful in these kinds of problems in which the relations between the parameters are not exactly known and can only be achieved by numerical methods. As the validation mean square error of the ANN is so close to zero, the trained network could be used to predict permeability for the fracture parameters other than the ones used for training the network. By this way permeability values could be determined without running the lattice Boltzmann simulation.

CHAPTER 6

CONCLUSION

Lattice Boltzmann method is based on Cellular Automata theory. It uses digital images of the medium to simulate fluid flow in order to obtain fracture permeabilities of two-dimensional synthetic fractures created using a fractal technique. Permeability values are obtained with lattice Boltzmann simulations for different fractal dimensions, anisotropy factors and mismatch lengths. The results of the simulations are initially analyzed using simple correlations and then by using the Artificial Neural Networks. Both correlation results and ANN analyses of the simulation data agrees with each other. In conclusion,

- In all cases it was observed that velocity increased at locations where the fracture aperture decreased along the fracture.

- There is a linear relationship between permeability and mean aperture –fractal dimension ratio as well as the mismatch length. However, the relationship is second order for anisotropy factor.

- By using the simulation outputs cubic law is modified and usage of an exponent larger than two is suggested.

- ANN is trained with validation mean square error value near to zero and used to verify the correlations obtained.

- ANN results showed that anisotropy of the fracture has more influence on the fracture permeability than the fractal dimension and the mean fracture aperture.

CHAPTER 7

RECOMMENDATION

The usage of the lattice Boltzmann method starts a new era for the field of petrophysics. The term “Virtual Rock Physics Laboratory” entered the scientific literature and the usage of the LBM is not only limited with the subject of this thesis. Three dimensional or multiphase applications could also be possible both in fractured and porous media. This method can be used to perform virtual experiments, and to understand the changes in the fluid flow characteristics in the rock according to the changes in the rock geometry. Because of it is particle based nature and capability of handling complex geometries it is defined as one of the best simulation tools for porous and fractured media.

REFERENCES

1. Amyx, J., Bass, D., Whiting, R., "Petroleum Reservoir Engineering", McGraw-Hill Book Company, 1960.
2. Witherspoon, P. A., Wang, J. S. Y., Iwai, K., Gale, J. E., "Validity of the Cubic Law for Fluid Flow in a Deformable Rock Fracture", Water Resources Research, 16, 1016, 1980.
3. Walsh, J. B., Brace, B. F., "The Effect of Pore Pressure on Porosity and the Transport Properties of Rock", J. Geophys. Res., B89, 9425, 1984.
4. Golf-Ract, Van, T. D., "Fundamentals of Fractured Reservoir Engineering", Elsevier Publishing Company, 1982.
5. Anderson, D. A., Tannehill, J. C., Pletcher, R. H., "Computational Fluid Mechanics and Heat Transfer", Hemisphere Publishing Company, 1984.
6. Succi, S., "The Lattice Boltzmann Equation for Fluid Dynamics and Beyond", Oxford University Press, 2001.
7. Bernsdorf, J., Durst, F., Schafer, M., "Comparison of Cellular Automata and Finite Volume Techniques for Simulation of Incompressible Flows in Complex Geometries", Int. J. Numer. Meth. Fluids 29: 251-264, 1999.
8. Abbott, M. B., Basco D. R., "Computational Fluid Dynamics, an Introduction for Engineers", Longman Scientific and Technical, 1989.
9. Luo, L. S., "The Lattice-Gas and Lattice-Boltzmann Methods: Past, Present, and Future", the 4th International Conference on Applied Computational Fluid Dynamics, Beijing, China, 2000.

10. Chen, H., Teixeira, C., Molvig, K., “Digital Physics Approach to Computational Fluid Dynamics: Some Basic Theoretical Features”, Intl. Jour. of Modern Physics C, 2000.
11. Sahimi, M., “Flow and Transport in Porous Media and Fractures Rock”, VCH Press, 1995.
12. Neumann, J. V., “Theory of Self-Reproducing Automata”, University of Illinois Press, 1966.
13. Wolfram, S., “Universality and Complexity in Cellular Automata”, Physica D, 10, 1-35, 1984.
14. Wolf-Gladrow, D., “Lattice-Gas Cellular Automata and Lattice Boltzmann Models: An Introduction”, Lecture Notes in Mathematics, Springer Press, 2000.
15. Ilachinski, A., “Cellular Automata, a Discrete Universe”, World Scientifc Publication, 2001.
16. Frisch, U., Hasslacher, B., Pomeau, Y., “Lattice Gas Automata for the Navier-Stokes Equations”, Phys. Rev. Lett. 56, 1505, 1986.
17. McNamara, G., Zanetti, G., “Use of the Boltzmann Equation to Simulate Lattice-Gas Automata”, Phys. Rev. Lett. 61, 2332-2335, 1988.
18. Keehm, Y., “Computational Rock Physics: Transport Properties in Porous Media and Applications”, PhD Thesis, Stanford University Department of Geophysics, 2003.
19. Succi, S., Foti, E., Higuera, F., “Three-Dimensional Flows in Complex Geometries with Lattice Boltzmann Method”, Europhysics Letters, 10(5): 433-438, 1989.
20. Guo, Z., Shi, B., Wang, N., “Lattice BGK Model for Incompressible Navier-Stokes Equation”, Journal of Computational Physics 165, 288-306, 2000.
21. Kumar, R., Sriram, S., Nivarthi, H., Davis, T., Kroll, D. M., Maier, R. S., “Application of the Lattice-Boltzmann Method to Study Flow and Dispersion in Channels with and without Expansion and Contraction Geometry”, Int. J. Numer. Meth. Fluids 31: 801-819, 1999.

22. Feder, J., “Fractals”, Plenum Press, NY, 1988.
23. Glover, P. W. J., Matsuki, K., Hikima, R., Hayashi, K., “Synthetic Rough Fractures in Rocks”, J. Geophys. Res., 103, B5, 9609-9620, 1998.
24. Amedei, B., Illangsekare, T., “A Mathematical Model for Flow and Transport in Non-Homogeneous Rock Fractures”, Int. J. Rock Mech. Min. Sci. Geomech. Abstr., 31, 719-731, 1994.
25. Deutsch C. V. Journel, A. G. “GSLIB: Geostatistical Software Library and User's Guide”, Oxford University Press, New York, 61-116, 1992.
26. Hecht-Neilsen, R., “Neurocomputing”, Addison-Wesley Publishing Company, Reading, MA, 1990.
27. Haykin, S. S., “Neural Networks- A Comprehensive Foundation” Prentice-Hall International, London, 1994.
28. Zhang, X., Knackstedt, M.A., Sahimi, M. “Fluid Flow across Mass Fractals and Self-Affine Surfaces”, Physica A, 233, 835, 1996.
29. Madadi, M., Sahimi, M., “Lattice Boltzmann Simulation of Fluid Flow in Fracture Networks with Rough, Self-Affine Fractures”, Physical Review E, 67, 026309, 2003.
30. Brown, S.R., “Simple Mathematical Model of a Rough Fracture”, J. Geophys. Res., 100, 5941-5952, 1995.

APPENDIX A

TABLES

Table A.1- LBM Simulation Outputs for Anisotropy Factor 1.0

LB-Perm (md)	Frac-Dim	Anisotropy-Fac	Mean-Aper (mm)	Image Porosity
1,591330E+06	2,21	1,00	1,3443	0,242404
1,682210E+06	2,25	1,00	1,455	0,255069
1,811020E+06	2,30	1,00	1,6051	0,271033
1,861850E+06	2,32	1,00	1,6691	0,278085
1,941310E+06	2,35	1,00	1,7693	0,287668
2,016380E+06	2,38	1,00	1,8746	0,298043
2,053540E+06	2,40	1,00	1,9478	0,304907
2,182700E+06	2,45	1,00	2,1411	0,321616
2,232300E+06	2,47	1,00	2,2224	0,328001
2,294030E+06	2,50	1,00	2,3486	0,337644

Table A.2- LBM Simulation Outputs for Anisotropy Factor 1.20

LB-Perm (md)	Frac-Dim	Anisotropy-Fac	Mean-Aper (mm)	Image Porosity
1,515140E+06	2,21	1,20	1,3673	0,245168
1,598570E+06	2,25	1,20	1,4777	0,257696
1,708540E+06	2,30	1,20	1,6276	0,273905
1,746250E+06	2,32	1,20	1,6913	0,280436
1,811460E+06	2,35	1,20	1,7912	0,289841
1,877930E+06	2,38	1,20	1,8962	0,29962
1,926930E+06	2,40	1,20	1,969	0,306342
2,036190E+06	2,45	1,20	2,1612	0,322744
2,064440E+06	2,47	1,20	2,242	0,328922

Table A.3- LBM Simulation Outputs for Anisotropy Factor 1.30

LB-Perm (md)	Frac-Dim	Anisotropy-Fac	Mean-Aper (mm)	Image Porosity
1,563810E+06	2,25	1,30	1,4925	0,259885
1,655990E+06	2,30	1,30	1,642	0,275424
1,708000E+06	2,32	1,30	1,7055	0,281829
1,749080E+06	2,35	1,30	1,805	0,291155
1,811680E+06	2,38	1,30	1,9096	0,300803

Table A.4- LBM Simulation Outputs for Anisotropy Factor 1.35

LB-Perm (md)	Frac-Dim	Anisotropy-Fac	Mean-Aper (mm)	Image Porosity
1,458550E+06	2,21	1,35	1,3903	0,248921
1,533000E+06	2,25	1,35	1,5005	0,261259
1,630050E+06	2,30	1,35	1,6497	0,276229
1,657380E+06	2,32	1,35	1,7132	0,282661
1,733670E+06	2,35	1,35	1,8125	0,291899
1,780480E+06	2,38	1,35	1,9168	0,30144
1,817500E+06	2,40	1,35	1,9891	0,307049

Table A.5- LBM Simulation Outputs for Anisotropy Factor 1.40

LB-Perm (md)	Frac-Dim	Anisotropy-Fac	Mean-Aper (mm)	Image Porosity
1,429650E+06	2,21	1,40	1,3988	0,249947
1,509930E+06	2,25	1,40	1,5088	0,262192
1,587070E+06	2,30	1,40	1,6578	0,277176
1,642220E+06	2,32	1,40	1,7211	0,283478
1,698700E+06	2,35	1,40	1,8202	0,292636
1,745750E+06	2,38	1,40	1,9242	0,301652
1,775580E+06	2,40	1,40	1,9964	0,307669
1,863760E+06	2,45	1,40	2,1866	0,323131

Table A.6- LBM Simulation Outputs for Anisotropy Factor 1.50

LB-Perm (md)	Frac-Dim	Anisotropy-Fac	Mean-Aper (mm)	Image Porosity
1,399950E+06	2,21	1,50	1,4165	0,252305
1,464130E+06	2,25	1,50	1,5262	0,263956
1,550940E+06	2,30	1,50	1,6747	0,27903
1,577710E+06	2,32	1,50	1,7377	0,284831
1,632680E+06	2,35	1,50	1,8363	0,293854
1,679810E+06	2,38	1,50	1,9398	0,302699

Table A.7- LBM Simulation Outputs for Anisotropy Factor 1.60

LB-Perm (md)	Frac-Dim	Anisotropy-Fac	Mean-Aper (mm)	Image Porosity
1,347420E+06	2,21	1,60	1,4351	0,254228
1,417880E+06	2,25	1,60	1,5444	0,265698
1,488010E+00	2,30	1,60	1,6923	0,280635
1,525730E+06	2,32	1,60	1,755	0,286278
1,568740E+06	2,35	1,60	1,8531	0,295142
1,621490E+06	2,38	1,60	1,956	0,303795
1,648170E+06	2,40	1,60	2,0273	0,310062

Table A.8- LBM Simulation Outputs for Anisotropy Factor 1.80

LB-Perm (md)	Frac-Dim	Anisotropy-Fac	Mean-Aper (mm)	Image Porosity
1,284310E+06	2,21	1,80	1,476	0,259665
1,334540E+06	2,25	1,80	1,5825	0,270421
1,404140E+06	2,30	1,80	1,729	0,28433
1,429170E+06	2,32	1,80	1,791	0,289308
1,460600E+06	2,35	1,80	1,8879	0,297811
1,500950E+06	2,38	1,80	1,9909	0,306843
1,538150E+06	2,40	1,80	2,0683	0,312466

Table A.9- LBM Simulation Outputs for Anisotropy Factor 2.50

LB-Perm (md)	Frac-Dim	Anisotropy-Fac	Mean-Aper (mm)	Image Porosity
1,162740E+06	2,21	2,50	1,6736	0,284111
1,211290E+06	2,25	2,50	1,7860	0,294246
1,258040E+06	2,30	2,50	1,9382	0,306743
1,283380E+06	2,32	2,50	2,003	0,312115
1,318030E+06	2,35	2,50	2,1045	0,319485
1,337510E+06	2,38	2,50	2,2114	0,327759

Table A.10- LBM Simulation Outputs for Anisotropy Factor 3.0

LB-Perm (md)	Frac-Dim	Anisotropy-Fac	Mean-Aper (mm)	Image Porosity
1,108740E+06	2,21	3,00	1,8139	0,301357
1,146230E+06	2,25	3,00	1,9238	0,310401
1,172860E+06	2,30	3,00	2,0753	0,321377
1,200720E+06	2,32	3,00	2,1418	0,326653
1,216610E+06	2,35	3,00	2,2456	0,333863
1,247500E+06	2,38	3,00	2,3541	0,340869

APPENDIX B

ALGORITHM

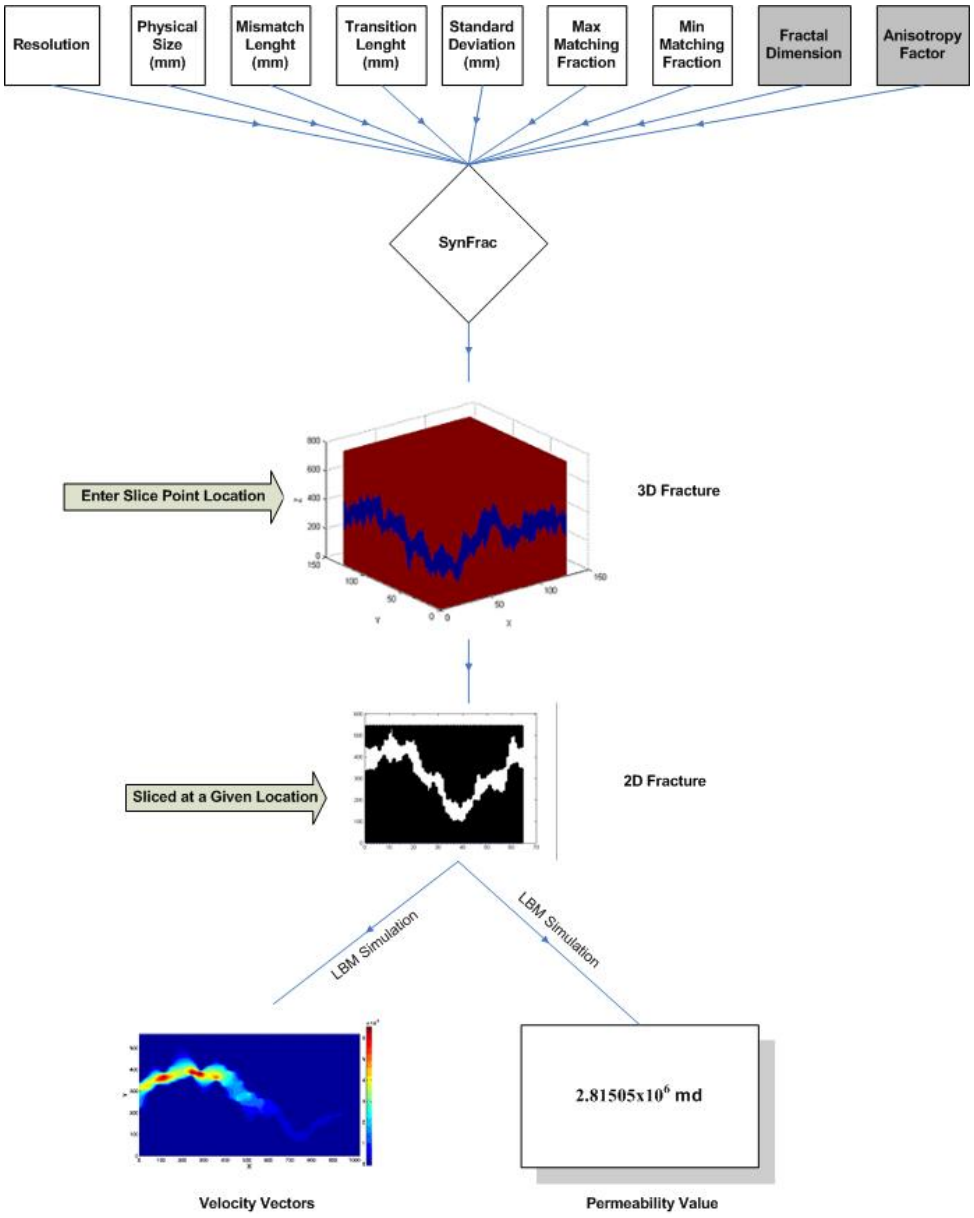

Figure B.1 - Steps of Fracture Generation and LBM Runs.

Code B.2 – Matlab Code for the Steps at Figure B.1

```
fracture_size=1024;
load frac3d.fre;

top2d=zeros(fracture_size,fracture_size);
bottom2d=zeros(fracture_size,fracture_size);


x=frac3d(:,1);
y=frac3d(:,2);
top=frac3d(:,3);
bottom=frac3d(:,4);
aper=frac3d(:,5);

up=rounddec(top,2)*100;
down=rounddec(bottom,2)*100;

slicepoint=input('Enter the x point to slice the fracture: ');

m=1;
for i=1:fracture_size
   for j=1:fracture_size
      if(x((i-1)*fracture_size+j)==slicepoint)
         upslice(m)=up((i-1)*fracture_size+j); m=m+1;
      end
   end
end
upslice=transpose(upslice);

n=1;
for i=1:fracture_size
   for j=1:fracture_size
      if(x((i-1)*fracture_size+j)==slicepoint)
         downslice(n)=down((i-1)*fracture_size+j); n=n+1;
```

```
      end
   end
end
downslice=transpose(downslice);


p=1;
for i=1:fracture_size
   for j=1:fracture_size
      if(x((i-1)*fracture_size+j)==slicepoint)
         aperslice(p)=aper((i-1)*fracture_size+j); p=p+1;
      end
   end
end
aperslice=transpose(aperslice);

mean_aperture=mean(aperslice);
disp(['Mean-Aperture of the Sliced Fracture (mm) = ',num2str(mean_aperture)]);

subplot(2,2,1);
plot(upslice);
hold on;
plot(downslice);
axis image;

for i=1:fracture_size
   for j=1:fracture_size
      top2d(i,j)=top((i-1)*fracture_size+j);
   end
end

for i=1:fracture_size
   for j=1:fracture_size
      bottom2d(i,j)=bottom((i-1)*fracture_size+j);
   end
end
```

```
%////////////////////////////////////////////////////////////////////////
%////////////////// 2D dimensions//////////////////////////////////////
%////////////////////////////////////////////////////////////////////////
min_down=int32(min(downslice));
max_up=max(upslice);

disp('----------Grid Size----------');
disp(['x-axis = ',num2str(fracture_size)])
disp(['y-axis = ',num2str(max_up-min_down)])
disp('----------Generating 2D Lattice Boltzmann Binary Input File----------');
lb2d_binary_data=zeros(fracture_size,max_up-min_down);
numberofones(i)=0.0;
for i=1:fracture_size
   for j=min_down:max_up

      if(upslice(i,1)<=j)
         lb2d_binary_data(i,j+1-min_down)=1;
         numberofones(i)=numberofones(i)+1;

      end

      if(j<=downslice(i,1))
         lb2d_binary_data(i,j+1-min_down)=1;
         numberofones(i)=numberofones(i)+1;

      end
   end
end
numberofones=transpose(numberofones);


disp('----------Binary Input File Generated----------');
disp('----------Drawing Fracture by Binary Data----------');
```

```
subplot(2,2,2);
imagesc(lb2d_binary_data);
axis image;
colorbar;
disp('----------Finding Permeability With LB2D Code----------');
numberofzeros=(max(upslice)-min(downslice))-numberofones;
gridspacing=mean_aperture/mean(numberofzeros);
disp(['Gridspacing is calculated as (mm) = ',num2str(gridspacing)]);
newaperture=numberofzeros*gridspacing;
new_mean_aperture=mean(newaperture);
disp('----------Calculating NEW MEAN APERTURE of the Sliced Fracture----------');
disp('----------New_Mean_Aperture=Grid_Spacing*Number_of_Zero_Grids(y-axis)---------');
disp(['NEW Mean-Aperture of the Sliced Fracture (mm) = ',num2str(new_mean_aperture)]);
perm2=perm2d(lb2d_binary_data,gridspacing);
subplot(2,2,4);
imagesc(perm2(:,:,1));
axis image;
colorbar;
```